

Supplementary Materials for

Taming the strength of interfacial interactions via nanoconfinement

David Nieto Simavilla, Weide Huang, Caroline Housmans, Michele Sferrazza and
Simone Napolitano* .

Correspondence to: snapolit@ulb.ac.be

This PDF file includes:

Materials and Methods
Supplementary Text
Figs. S1 to S12
Table S1

MATERIALS AND METHODS

No unexpected or unusually high safety hazards were encountered in the preparation and characterisation of our samples.

1.1 Preparation of single polymer layer systems

Thin films of polystyrene (PS), poly(methyl methacrylate) (PMMA), poly(4-tert butylstyrene) (PtBS), and poly(4-methylstyrene) (P4MS) were prepared by spincoating dilute polymer solutions onto silicon wafer substrates, covered by a native oxide layer of ~ 2 nm. PS, PtBS and P4MS were dissolved in toluene ($>99\%$ purity), while PMMA was dissolved in benzene ($>99\%$ purity). Before spincoating, wafers were rinsed with a series of appropriate solvents (typically acetone followed by isopropanol and finally toluene, or in the case of PMMA samples benzene). Details on the polydispersity and source of the polymers used in this study are presented in Table S1. The thickness of the deposited layers is controlled by changing the concentration of the polymer solution while spinning rate is kept constant at 4000 rpm. The thickness of the spincoated polymer layers L ranged from 10 to 500 nm. Depending on the molecular weight of each specific polymer, these thicknesses values were chosen to cover the interval $2R_g < L < 30R_g$. This choice allowed us to investigate the effect of nanoconfinement over a broad thickness range. The measured adsorbed layers range from 3 to 15 nm. Note that films below ~ 3 nm are intrinsically unstable and they spontaneously dewet, via spinodal decomposition.¹

After spincoating, thin films relax due changes in the microscopic structure upon evaporation of residual solvent. These phenomena induce a time dependent reduction in film thickness. Following previous work, to allow for structural relaxation²⁻³ and reach a stable value of L , our films are dried in vacuum for 20 minutes and pre-annealed above the glass transition temperature for 10 minutes, which is over a thousand times larger than the structural relaxation time. The spincoated film thickness was determined via ellipsometry (MM-16, Horiba),⁴⁻⁵ see 1.4.

1.2 Preparation of polymer bilayer systems

For the experiments in Figure 2E, we prepared series of multilayers of the type Air/PMMA/PS/SiO₂/Si. PMMA/PS bilayers have been widely investigated,⁶⁻⁷ which permitted an easy and reliable fabrication routine: 1) we prepared single polymer layers of the type Air/PS/SiO₂/Si following the procedure described above; 2) we spin-coated solutions of PMMA in acetic acid directly onto the PS films – as polystyrene is not soluble in acetic acid, the previously spincoated films of PS are not affected by the deposition of the upper layer; 3) the samples are again dried in vacuum for 20 min and pre-annealed as described above.

1.3 Adsorption experiments

Samples were annealed on a hot plate (STUART SD160, with a temperature stability of 0.1 K), from 0 to 72 hours, depending on the system investigated, to allow for adsorption

of polymer chains onto the substrate (see Figures 1D and S2 for examples of adsorption kinetics). After annealing, non-adsorbed polymer chains are washed off reproducing Guiselin's experiment:⁸ samples were rinsed and soaked for 1 hour in the same good solvent used to prepare the spin-coated solutions (due to an intrinsically lower solubility of PMMA in benzene, samples are soaked for 3 hours⁹), in a one-step for the monolayer samples and a two-step (first in acetic acid, then in toluene) protocol for the bilayer samples. The thickness of the adsorbed layer, h_{ads} , was measured using ellipsometry (MM-16, Horiba),⁴⁻⁵ see **1.4**.

1.4 Determination of L and h_{ads} via ellipsometry

The deposited spincoated thickness L and the adsorbed polymer layer thickness h_{ads} are measured using ellipsometry (MM-16, Horiba). The thin film polymer monolayer (Air/Polymer1/SiO₂/Si) and bilayer (Air/Polymer2/Polymer1/SiO₂/Si) systems are modeled as a multilayer Cauchy model to fit the spectroscopic angles Ψ and Δ at wavelengths λ between 430 and 850 nm¹⁰. Film thickness is obtained by fitting the ellipsometric angles to a model considering bulk optical properties¹¹. To accurately determine the different thicknesses in the system a step-by-step process is followed in which the thickness of the underlying layer gets determined before the deposition of the successive capping layer. For example, for the system Air/PS/SiO₂/Si the SiO₂ layer thickness is measured before spincoating the polymer, using the bare substrate and fitting the oxide layer thickness to the optical model Air/SiO₂/Si; the obtained value of the thickness of SiO₂ is then fixed while fitting the PS layer thickness, in the monolayer systems. Similarly, for the bilayer systems the thickness of the SiO₂ and that of PS (Polymer1) are measured following the same procedure as above and then fixed, while fitting the thickness of the PMMA (Polymer2) layer. Thickness of the SiO₂ layer was found to vary from 1.5 to 2.5 nm. Spincoated polymer layer thickness L range roughly from 10 to 500 nm and is chosen depending on the molecular weight of each specific polymer to cover the range of interest. The measured adsorbed layers range from 3 to 15 nm. Note that, in agreement with the scheme presented in the main text and in **2.2**, films below ~ 3 nm are intrinsically unstable (i.e. have a positive A_{eff}) and spinodally dewet.¹

The thickness of the adsorbed layers, h_{ads} , was measured following the same procedure indicated above for single layers, using bulk values for the optical parameters of the bulk layer. We expect the error induced by this choice to be on the order of the density difference between adsorbed and not adsorbed state, that is smaller than experimental uncertainty ($\approx 5\%$). To further prove the validity of this assumption, for a selection of samples covering the whole investigated range of h_{ads} we had considered comparison of the thickness value obtained via ellipsometry with that determined via atomic force microscopy (AFM), as the height of steps obtained by removing the organic layer with a soft sharp pen. Comparison of the values found via AFM with those measured via ellipsometry confirmed our assumption and validated the optical model:^{4-5, 12-13} slopes of linear fits to plots of the two independent measurements (i.e. h_{ads} via ellipsometry *versus* h_{ads} via AFM) deviate from 1.00 by less than 5%.

1.5 Determination of the adsorbed amount Γ^∞

The thickness of the irreversible adsorbed layer, h_{ads} , is directly proportional to adsorbed mass Γ_{m} , that is, the total mass of all the monomers directly (those pinning on the substrate) and indirectly (those connected to pinned monomers) irreversibly adsorbed, per unit area

$$h_{\text{ads}} = \frac{\int_0^\infty \Gamma_{\text{m}}(z) dz}{\rho_{\text{ads}}} \quad (\text{S1})$$

where ρ_{ads} is the density of the adsorbed layer, which, following our optical model and its validation, can be approximated with the density of the bulk, ρ . Considering the extremely low surface roughness of adsorbed layers (3 – 4 Å),¹⁴ S1 simplifies to

$$h_{\text{ads}} = \frac{\Gamma_{\text{m}}}{\rho} \quad (\text{S2})$$

Considering that the number of contacts a chain makes with a flat substrate increases with $N^{-1/2}$, with N the polymerization degree, the number of molecules adsorbed per unit area, Γ , is given by

$$\Gamma = \frac{\rho h_{\text{ads}}}{N_{\text{A}}} N^{1/2} \approx \frac{\rho h_{\text{ads}}}{N_{\text{A}}} \left(\frac{M_{\text{w}}}{m_{\text{m}}} \right)^{1/2} \quad (\text{S3})$$

where N_{A} is the Avogadro number, M_{w} is the average molar mass and m_{m} is the mass of one monomer; the approximation $N \approx M_{\text{w}}/m_{\text{m}}$ is valid for monodisperse chains long enough to consider negligible the difference in mass between inner monomers and chain ends.

Equation S3 is valid at any time during the formation of the adsorbed layer. More specifically, after long enough annealing times, adsorption reaches an equilibrium state and Eq S3 can be written as,

$$\Gamma^\infty = \frac{\rho h_{\text{ads}}^\infty}{N_{\text{A}}} \left(\frac{M_{\text{w}}}{m_{\text{m}}} \right)^{1/2} \quad (\text{S4})$$

where we have used the superscript “ ∞ ” to indicate the equilibrium state. Introducing in S4 a dependence on the thickness of the spincoated film, L , we get

$$\Gamma^\infty(L) = \frac{\rho h_{\text{ads}}^\infty(L)}{N_{\text{A}}} \left(\frac{M_{\text{w}}}{m_{\text{m}}} \right)^{1/2} \quad (\text{S5})$$

Considering that each macromolecule makes in average the same number of contacts with the substrate, the total number of contacts between macromolecules and substrate per unit area, n , is directly proportional to Γ . Therefore, from Eq S5 we obtain the relation used to generate the results in Figures 1 and 2,

$$\frac{\Gamma^\infty(L)}{\Gamma_{\text{bulk}}^\infty} = \frac{n^\infty(L)}{n_{\text{bulk}}^\infty} = \frac{h^\infty(L)}{h_{\text{bulk}}^\infty} \quad (\text{S6})$$

where we have use the subscript “bulk” to indicate bulk properties (i.e. $L > 7 - 10R_{\text{g}}$).

1.6 Kinetics of irreversible adsorption, data handling and fitting to the kinetic model

At short times, the thickness of the adsorbed layer increases linearly with time,⁴

$$h_{\text{ads}}(t) = vt \quad \text{for } t < t_{\text{cross}} \quad (\text{S7})$$

where $v \propto q\Phi$, q is the monomer adsorption rate and Φ is the product of bulk density and $N^{1/2}$, where N is the polymerization number. A formal derivation of Eq S7 can be found in reference.¹⁵ At later times, although the mechanism of adsorption is unaltered, the rate of adsorption gradually drops due to surface crowding. This second regime is described by,¹⁵

$$h_{\text{ads}} = h^\infty + \ln \left[1 - A \exp\left(-\frac{t-t_{\text{cross}}}{\tau}\right) \right] \quad \text{for } t > t_{\text{cross}} \quad (\text{S8})$$

where $A = 1 - \exp(-(h^\infty - h_{\text{cross}})) \approx 1$ and $\tau = [\exp(-h^\infty)\Phi Cq]^{-1}$. For thick films, we carefully verified that C is a temperature independent constant¹⁵ and that Eq S8 is valid for all the polymers investigated in this work.

Kinetics data sets covering a time scale from 0 to 72h are simultaneously fitted to Eq S7 and Eq S8 through an iterative method that provides the crossover point $(t_{\text{cross}}, h_{\text{cross}})$ (i.e. the transition point between regimes) and determines the kinetic parameters v , h_L^∞ , and τ ¹³. Finally, we perform control tests on the fit results to discard unphysical conditions, as for example growth rates in the logarithmic regime being larger than in the linear regime. Examples of fits to Eq S7 and Eq S8 are included in Fig S1, as well as in Fig 1F.

The value of h_L^∞ can be determined as a fitting parameter to Eq S8, that is via analysis of the whole kinetics, or, directly, and with high accuracy, by averaging the values of h_{ads} obtained in measurements at times $t \gg \tau$ (See Fig S3). Note that to use the second procedure proper characterization of the whole kinetics covering the thickness range is required, (i.e. the value of τ needs to be determined).

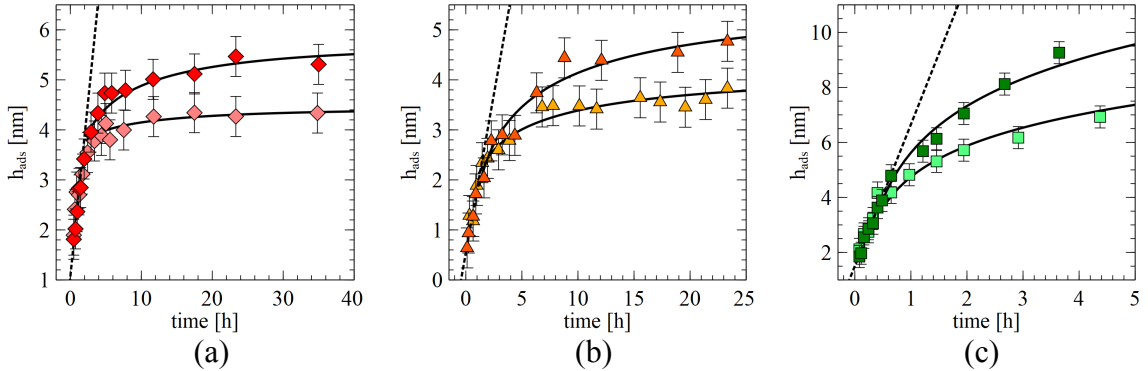


Fig. S1 - Adsorption kinetics for monolayer films: (a) PtBS74, $L = 180$ nm (dark red diamonds) and $L = 29$ nm (light red diamonds), (b) PMMA350, $L = 120$ nm (dark orange triangles) and $L = 42$ nm (light orange triangles) and (c) P4MS72, $L = 74$ nm (dark red diamonds) and $L = 17$ nm (light red diamonds). For all the polymers, the kinetics are well described by a linear region (dashed lines, Eq. (S7)) followed by slow-down in the kinetics (solid lines, Eq. (S8)).

SUPPLEMENTARY TEXT

2.1 Effect of nanoconfinement on the kinetics of irreversible adsorption

As shown by data in Figures 1F, S3 and S4, at short timescales the kinetics of adsorption is not affected by nanoconfinement (i.e. no dependence on L), while a significant thickness dependence is observed at longer timescales. The results in Fig 1F for PS, together with those for other polymers in Fig S1, reveal that for $2R_g < L < L_0$:

$$\partial h_{\text{ads}}/\partial L|_{t < t_{\text{cross}}} = 0 \quad (\text{S9a})$$

$$\partial h_{\text{ads}}/\partial L|_{t > t_{\text{cross}}} < 0 \quad (\text{S9b})$$

$$\partial t_{\text{cross}}/\partial L = \partial h_{\text{cross}}/\partial L = 0 \quad (\text{S9c})$$

To understand the molecular origins of this trend, we have considered how a change in L affects the physical quantities governing the kinetics of adsorption. We have thus analyzed the impact of changes in molecular mobility, adsorption reaction mechanism, density and interfacial potential on $h_{\text{ads}}(t)$.

Monomer reaction rate q : We have shown that the activation energy of v (and thus of q), for the polymer/substrate systems considered in this work, are on the order of 50-120 kJ/mol¹⁵. These values are similar to those of local molecular rearrangement, as those of β -relaxation processes.¹⁶ Based on these observations, we proposed that adsorption is an inefficient process requiring the repetition of a large number of events (eventually $> 10^9$) occurring at the timescale of molecular motion.¹⁷

A change in molecular dynamics induced by nanoconfinement could, therefore, alter the value of q (and thus v). Similarly, the value of q could be affected by a change in adsorption mechanism (e.g. due to an alteration of molecular rearrangements in the thinner films, which might ease or inhibit pinning onto the substrate). In Figure S2A we plotted the result of perturbations in the kinetics induced by changes in q by $\pm 20\%$. We remark that the pattern in Fig S2A does not resemble the experimental trends in $h_{\text{ads}}(t, L)$, see Fig 1F and Fig S1. A mere change in q cannot thus be explain the changes in $h_{\text{ads}}(t, L)$.

Density ρ : The density of thin polymer films differs from the value measured in bulk melts by not more than 1%.¹⁸⁻¹⁹ As this difference is smaller than the relative error on the determination of h_{ads} (2-10%), we conclude that the contribution of a change in density on $h_{\text{ads}}(t)$ is negligible and cannot explain the experimental trends in $h_{\text{ads}}(t, L)$. In Fig S2B we have shown an exaggerated change of 5% in Φ , which at constant molecular weight is only affected by density.

Interfacial potential ϵ_w : We have verified that, within experimental errors, the value of h^∞ is not affected by temperature, while v (and thus q) has large thermal activation energy (50-120 kJ mol⁻¹) (8). Simulation of the adsorption kinetics of polymer melts onto attractive interfaces have shown that the equilibrium adsorbed amount is strongly affected by the depth of the monomer-wall interaction potential, ϵ_w .^{15, 20} A linear correlation between the former and the latter parameter is found at small ϵ_w values, while saturation is reached above a threshold depth of the monomer-wall interaction potential.

Because above this value an increase in Γ requires a larger interfacial density, saturation is, intuitively, reached because of the finite compressibility of the material.

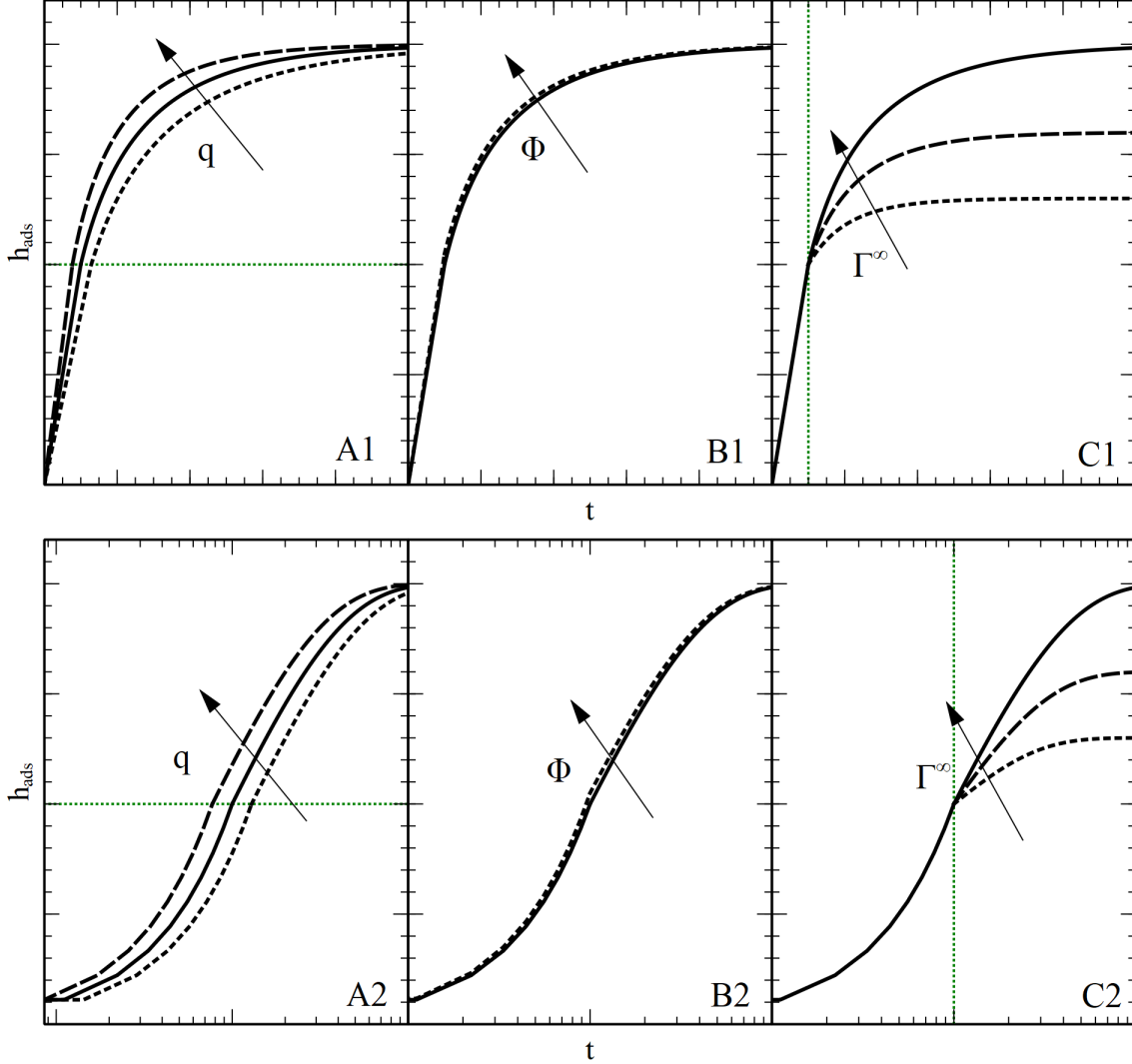


Fig. S2 - Representation of the two-regime model and the parameters that can be used to affect the kinetics and the equilibrium state. Top panels: Linear scale. Bottom panels: logarithmic scale. **A:** Kinetics associated with an increase/decrease in q (i.e. $\sim 1.2q$ dashed line and $\sim 0.8q$ dotted line) due to an increase/decrease in temperature of 5 K with an activation energy of 80 kJ/mol. **B:** Kinetics associated with changes in Φ due to increasing density by 5% (dotted). **C:** Kinetics associated with changes in h^∞ through changes in the interaction potential resulting in $0.8h^\infty$ (dashed) and $0.65h^\infty$. Note that the solid line represents the same reference kinetics in all panels given by q , Φ and h^∞ . The vertical or horizontal green dotted lines intersection with the different curves indicates $(h_{\text{cross}}, t_{\text{cross}})$, the transition between the linear and the logarithmic-exponential regime.

Importantly, this trend in $\Gamma^\infty(\varepsilon_w)$ resembles that of $\Gamma^\infty(L)$. In Figure S2C, we have thus considered how an arbitrary change in h_L^∞ , at constant q and Φ , affects $h_{\text{ads}}(t, L)$. The pattern in Figure S2C satisfies the criteria given by S9a-c and is in agreement with the observed experimental trends in $h_{\text{ads}}(t, L)$. We conclude that the results in Fig 1F and Fig S1 can be explained via the following relations:

$$\partial q \Phi / \partial L \approx \partial q / \partial L \approx 0 \quad (\text{S10a})$$

$$|\partial h_L^\infty / \partial L| \approx |\partial \epsilon_w / \partial L| = |\partial \Xi / \partial L| \quad (\text{S10b})$$

Relation S10a could be promptly verified by analyzing the thickness dependence of v (see Fig S3 and Fig S4).

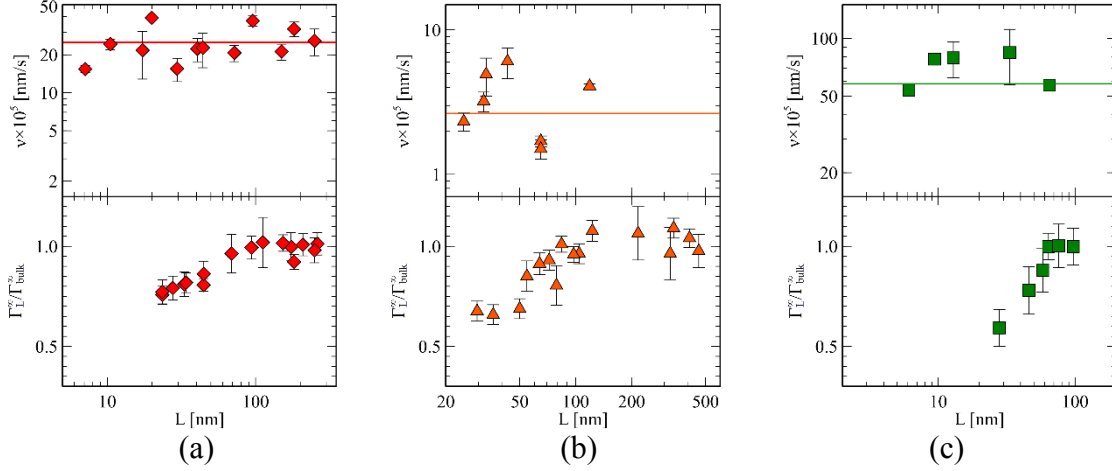


Fig. S3. - Linear regime adsorption rate v (top) and normalized equilibrium adsorbed amount $\Gamma_L^\infty / \Gamma_{\text{bulk}}^\infty$ (bottom) as a function of the spincoated thickness L for PtBS74 (a), PMMA350 (b) and P4MS72 (c). For all polymers, the adsorption rate in the linear regime is independent of L while the equilibrium adsorbed amount is affected by confinement.

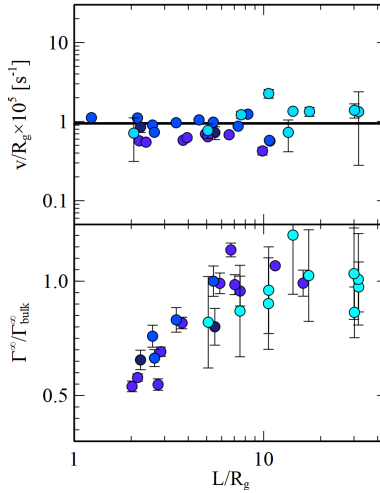


Fig. S4 - Normalized linear regime adsorption rate v/R_g and equilibrium adsorbed thickness $\Gamma^\infty / \Gamma_{\text{bulk}}^\infty$ as a function of the spincoated thickness L/R_g for PS 49k (light-blue), 325k, 560k, and 1460k (dark-purple), see Table S1 for a legend of colors. For all molecular weights, the adsorption rate in the linear regime is independent of L while the equilibrium adsorbed thickness is affected by confinement.

Experimental test of Eq S10b requires the existence of a material property Ξ ascribable to the interfacial potential having the same thickness dependence as ϵ_w and, whose absolute value is directly proportional to h^∞ . While searching for this material property, we discarded those components of the interfacial potential acting only on a short-range, e.g.

electronic and polar interactions, since those saturate at distances from the interface orders of magnitude smaller than those reported here.²¹ We have, hence, considered long-range components, as for example those related to dispersive (van der Waals) forces. The effective Hamaker constant A_{eff} , a conventional and straightforward way of measuring the magnitude of these long-range interactions, is thus an optimal candidate for Ξ . Fig 2A-E provide the experimental evidence of the validity of Eq S10b for $\Xi = A_{\text{eff}}$, that is, the changes in the adsorbed thickness with L are proportional to the changes in the Hamaker constant with L .

We remark that the thickness of the spincoated layer should be just considered as a functional parameter to vary the effective Hamaker constant, A_{eff} . Other quantities (e.g. the thickness and the chemical nature of the other layers, such as the thickness of the PMMA capping layer in the bilayer experiments of Fig. 2E, could be used to modify Γ^∞ in the thickness range where the Hamaker constant depends on the layer size. This point justifies the use of partial derivatives in Eq S9 and Eq S10.

We have verified, in fact, that it is possible to modify the thickness of the adsorbed layer (e.g. of PS on SiO_2) without changing the thickness of the adsorbing layer (L_{PS}) but that of a capping layer (L_{PMMA}) in multilayers systems (i.e. Air/PMMA/PS/ SiO_2/Si). A change in L_{PMMA} at constant L_{PS} permits to vary A_{eff} , see Fig S6. Remarkably, regardless of the sample geometry, the equilibrium adsorbed amount Γ^∞ depends only on the value of A_{eff} and not on the thickness of the single spincoated layers, see Fig S5.

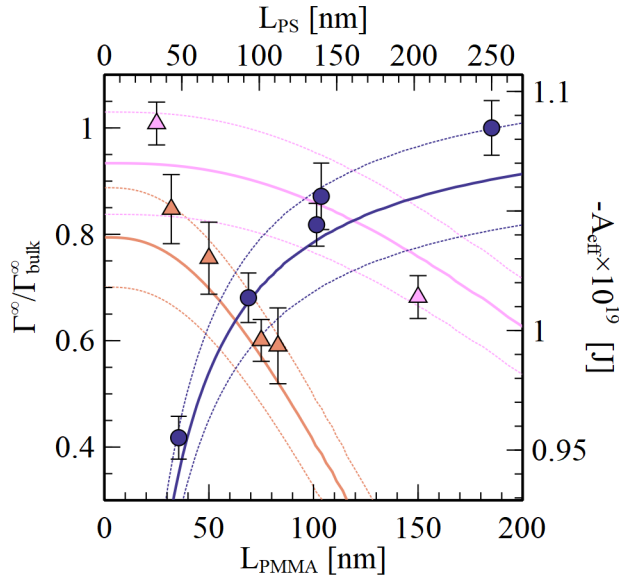


Fig. S5 - Normalized adsorbed amount as a function of the PMMA layer thickness for bilayers with $L_{\text{PS}} = 320\text{nm}$ (pink triangles) and $L_{\text{PS}} = 140\text{nm}$ (orange triangles), and as a function of the PS layer thickness for monolayer data (purple circles). The solid lines going through the data (linked to the secondary y-axis) show A_{eff} for the same systems (colors as in the experimental data), dotted lines indicate an error of $\pm 2\%$ error on the effective Hamaker constant. The vertical axis has been adjusted according to the relation between adsorbed amount and A_{eff} found in Figure 2E (i.e. $\Gamma^\infty/\Gamma_b^\infty = -3.9A_{\text{eff}} - 3.65$). Note that the same adjustment is valid for both bilayers and monolayers.

2.2 Calculation of the effective Hamaker constants

The Hamaker constants for the different systems presented in the main text have been obtained following the approach used in the literature.^{6, 21-22} This method is based on the estimation of the free energy of a system of parallel layers of known thickness. In this framework, the free energy of interaction due to long-range dispersion forces between two semi-infinite layers, separated by a distance L , is given by:

$$w(L) = -\frac{A_{ijk}}{12\pi L^2} \quad (\text{S11})$$

where A_{ijk} is the Hamaker constant between i and k layers separated by medium j . The Hamaker constant of this three-layer system can be calculated by combination of the Hamaker constants of the single materials (i.e. $A_{ijk} \approx (\sqrt{A_{ii}} - \sqrt{A_{jj}})(\sqrt{A_{kk}} - \sqrt{A_{jj}})$), where A_{ii} is the Hamaker constant of two layers of the same material separated by vacuum. Alternatively, a more accurate formula is given by,

$$A_{ijk} \approx \frac{3}{4} k_B T \left(\frac{\varepsilon_i - \varepsilon_j}{\varepsilon_i + \varepsilon_j} \right) \left(\frac{\varepsilon_k - \varepsilon_j}{\varepsilon_k + \varepsilon_j} \right) + \frac{3h\nu_e}{8\sqrt{2}} \frac{(n_i^2 - n_j^2)(n_k^2 - n_j^2)}{(n_i^2 + n_j^2)^{\frac{1}{2}}(n_k^2 + n_j^2)^{\frac{1}{2}} \left\{ (n_i^2 + n_j^2)^{\frac{1}{2}} + (n_k^2 - n_j^2)^{\frac{1}{2}} \right\}} \quad (\text{S12})$$

where ε is the dielectric constant for each media, n the refractive index, k_B and h the Boltzmann and Plank constants respectively, and ν_e is the main electronic adsorption frequency constant²¹ Note that, in systems such as the ones considered in this study, the first term in Eq S12, denominated as the zero-frequency term ($\nu = 0$), is typically one order of magnitude smaller than the second term ($\nu > 0$), and is, hence, usually neglected.

When considering systems with additional layers it is useful to introduce the concept of effective Hamaker constant (i.e. the effective interaction potential that gives a free energy in the form of Eq S11). In a system with 4 layers (i.e. Si/SiO₂/PS/Air \equiv 1/2/3/4) the free energy for layer 3, PS, is given by:

$$w_3(L_2, L_3) = -\frac{A_{234}}{12\pi L_3^2} - \frac{A_{134} - A_{234}}{12\pi(L_3 + L_2)^2} \quad (\text{S13})$$

where L_i is the thickness of the i th layer and the coefficient on the second term can be approximated by $A_{134} - A_{234} \approx (\sqrt{A_{44}} - \sqrt{A_{33}})(\sqrt{A_{11}} - \sqrt{A_{22}})$ ²¹ or more accurately calculated using S12. Under this scheme, the effective Hamaker constant acting on layer 3 is given by:

$$A_{\text{eff},3} = A_{234} + \frac{A_{134} - A_{234}}{(1 + L_2/L_3)^3} \quad (\text{S14})$$

Note that it is important to differentiate the material layer at which the Hamaker constant or the free energy is being calculated. For example, in a Si/PS/PMMA/Air \equiv 1/2/3/4 system, the free energy for the PS layer is given by:

$$w_2(L_2, L_3) = -\frac{A_{123}}{12\pi L_2^2} - \frac{A_{124} - A_{123}}{12\pi(L_2 + L_3)^2} \quad (\text{S15})$$

and the resulting effective Hamaker constant is given by:

$$A_{\text{eff},2} = A_{123} + \frac{A_{124} - A_{123}}{(1+L_3/L_2)^3} \quad (\text{S16})$$

Similarly, we can expand Eq S13 or Eq S15 to a system of 5 layers (i.e. Si/SiO₂/PS/PMMA/Air = 1/2/3/4/5) to obtain the following expression for the effective Hamaker constant of the PS layer:

$$A_{\text{eff},3} = A_{1235} + \frac{A_{1234} - A_{1235}}{(1+L_3/L_4)^3} \quad (\text{S17})$$

where the effective Hamaker constants of the 4 layers subsystems have been calculated using the analysis given by Eqs. S14 through S16. Examples of the evolution as a function of the different layer thicknesses for the monolayer and bilayer systems presented in this study are included in Figure S6.

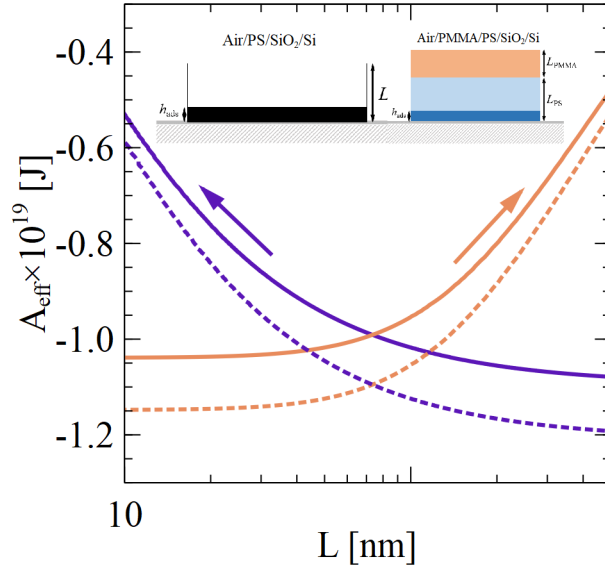


Fig. S6 - Effective Hamaker constant for a monolayer Air/PS/SiO₂/Si system as a function of the PS spin-coated layer thickness with a SiO₂ layer of 2 nm (purple). Effective Hamaker constant for a bilayer Air/PMMA/PS/SiO₂/Si system as a function of the PMMA spin-coated layer thickness for 140 nm PS layers with a 2 nm SiO₂ layer. The solid (dashed) lines indicate the retarded (non-retarded) effective Hamaker constant according to Section 2.2. The arrows indicate the directions in which the effective Hamaker constant is reduced by decreasing the thickness of the PS layer in monolayer systems and by increasing the thickness of the PMMA layer in bilayer experiments. A reduction in the absolute value of A_{eff} is, hence, induced by a decrease in the PS layer thickness in the case of monolayers, and by an increase in PMMA layer thickness in bilayers.

It is important to notice that Eq S14 and Eq S17 provide significantly different trends as a function of the thickness of the single layers. According to Eq S14, the absolute value of the effective Hamaker constant monotonically decreases when decreasing the thickness of the polymer layer in a monolayer system (i.e. it becomes less negative). On the contrary following Eq S17, a similar trend can be reached by increasing the thickness of the capping PMMA layer, while keeping that of the PS layer constant. As a result, both decreasing polymer thickness in monolayer systems and increasing capping polymer

layer thickness in bilayer systems yield a reduction of the absolute value of the effective Hamaker constant, and therefore a reduction of the equilibrium adsorbed layer thickness (See Fig S6 and Fig S12).

Considering that the relative error on the determination of the spincoated thickness L does not exceed 3%, the corresponding relative error on A_{eff} would be negligible. Taking into account the approximations behind Eqs S11 – S17, we have considered a 1% error in Hamaker constants of single layer systems, and 2% error for bilayers. We remark that the relative error on A_{eff} does not exceed that on Γ , and that the largest uncertainties in Figure 2 are thus given by the latter quantity.

2.2.1 Retardation effects on the effective Hamaker constant

The second term in Eq S10 is affected by retardation, due to the London component of van der Waals interactions, requiring a non-zero time to cover the layer thickness. The determination of the exact contribution of retardation effects on A_{eff} requires elaborate quantum mechanics calculations. However, considering the experimental uncertainties on the determination of L and h_{ads} , for our purposes a satisfactory correction to the Hamaker constant can be achieved by considering a correction factor:²³

$$f(L) = A_{v>0,\text{ret}}/A_{v>0,\text{non-ret}} = 1/(1 + b L/\lambda) \quad (\text{S18})$$

where the value of $b = 5.32$, is chosen in agreement with more detailed description of the London dispersion energy,²⁴ and the characteristic wavelength of the interaction $\lambda = \frac{c}{\nu_e} \sim 100$ nm, with c is the speed of light in the interaction media.

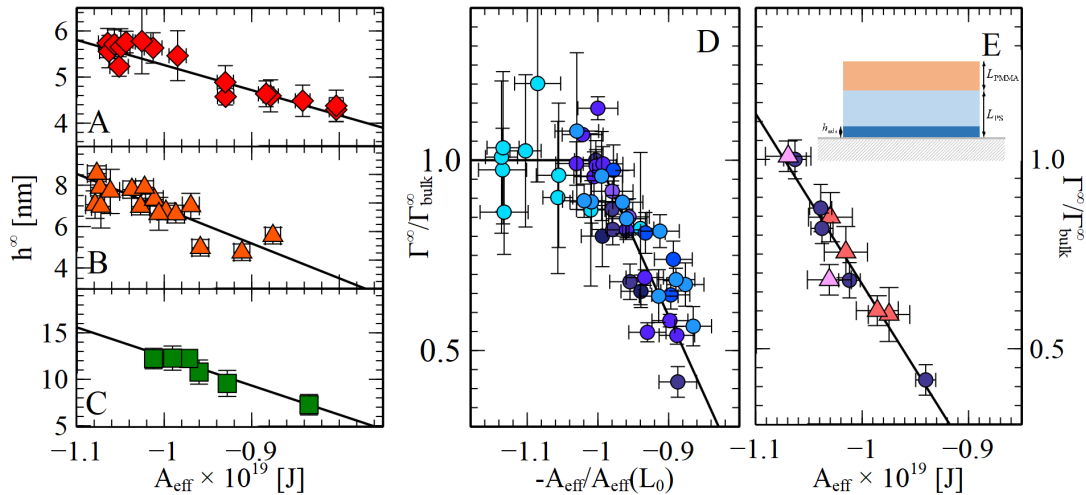


Fig. S7 - (A – C): Equilibrium adsorbed thickness for single layer systems (see sketch in Figure 1E) of PtBS74 (A, red diamonds), PMMA350 (B, orange triangles) and P4MS72 (C, green squares) as a function of the effective Hamaker constant (A_{eff}) acting at the polymer/substrate interface. Importantly, in this plot of the same adsorbed amount data of Figure 2, the values of the Hamaker constant have been corrected via Eq S18 to include retardation effects. (D) Equilibrium adsorbed amount normalized to bulk value as a function of the ratio $A_{\text{eff}}(L)/A_{\text{eff}}(L_0 = 7R_g)$ for thin films of PS of different molecular weight (same symbols as in Figure 1D). We remark that datasets of $\Gamma^\infty/\Gamma_{\text{bulk}}^\infty$ vs $A_{\text{eff}}(L)/L_0$ for different molecular weights do not collapse in a master plot, because $A_{\text{eff}}(L)$ is not a linear function of L . (E) Bilayer systems

(see sketch in the top right corner of the same panel): normalized adsorbed amount for layers PS1000 (320 nm pink triangles, 140 nm orange triangles) capped by thin layers of PMMA.

We verified that though retardation affects the value of A_{eff} , the linearity of $h_{\text{ads}}(A_{\text{eff}})$ remains unaltered (See Fig S7 which is an analogue to Fig 2 of the main text accounting for the effect of retardation in A_{eff}). Our reasoning is thus valid independently on the introduction of retardation effects. We furthermore remark that retardation does not affect the absolute value of $\partial h_{\text{ads}}/\partial A_{\text{eff}}$ (See Fig S8 and Fig S9). Due to the easier computation and simplicity, in the main text we show experimental data as a function of non-retarded Hamaker constants.

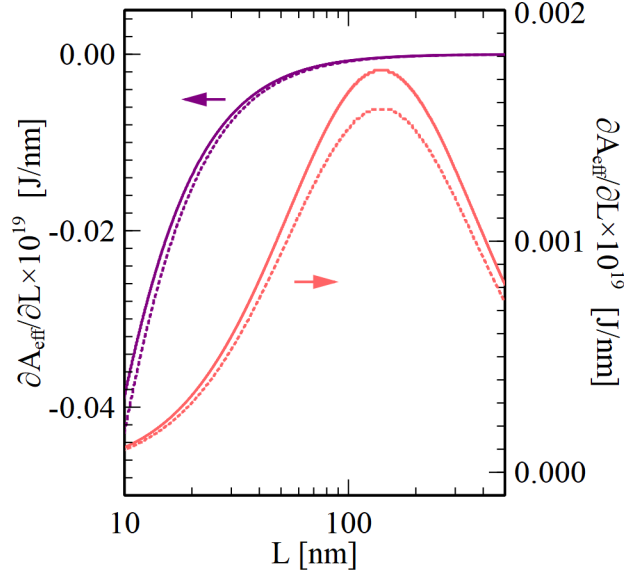


Fig. S8 – Partial derivative of the effective Hamaker constant with respect to the PS (PMMA) film thickness for monolayer (bilayer) systems in purple (orange). The effect of retardation is shown by the dashed lines.

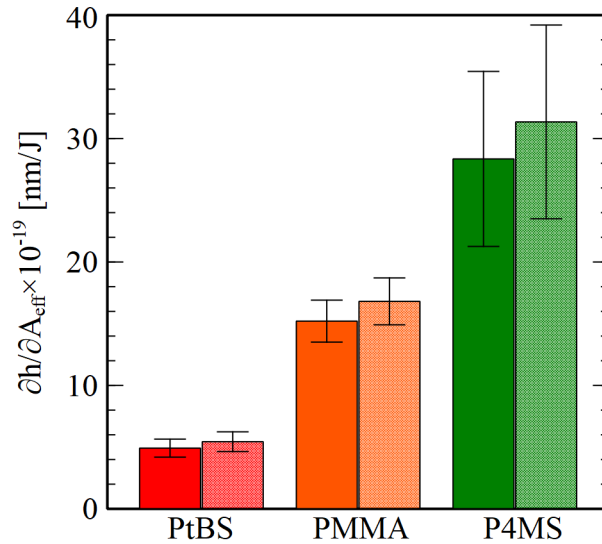


Fig. S9 – Summary of the effect of retardation in the estimation of the slope found in Figure 2A-C. Solid bars correspond to the use of non-retarded values of the effective Hamaker constant with the patterned bars with the same color correspond the same data analysis applied with retarded values of the effective Hamaker constant calculated using Eq S18.

SUPPLEMENTARY FIGURES

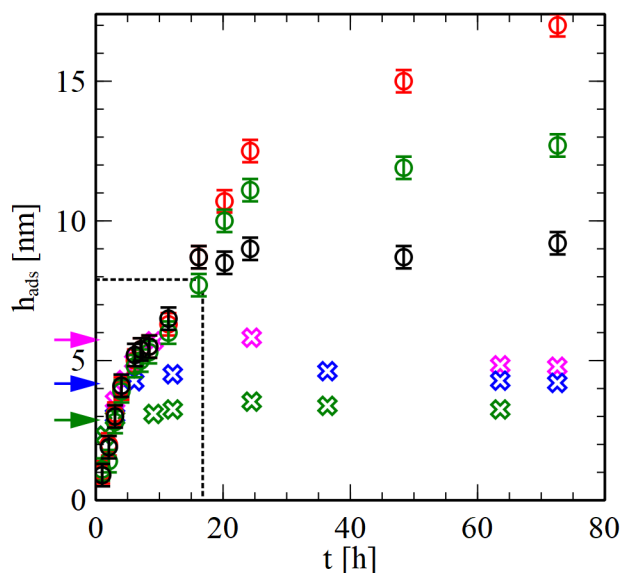


Fig. S10 - Adsorption kinetics for samples of PS325 of different layer thickness, $L = 134$ nm (red circles), 74 nm (green circles) and 35 nm (black circles), $L = 22$ nm (magenta crosses), 15 nm (blue crosses) and 9.6 nm (green crosses). coincide (marked dotted lines). For this molecular weight $R_g \sim 16$. For $L > 2R_g$ (circles), the crossover point (see marked dotted lines) is independent on L . For $L < 2R_g$ (crosses), deviation from the linear regime occurs at progressively shorter times and smaller thicknesses (see colored arrows). At longer times, due to depletion in available adsorbable material, the adsorbed layer thickness quickly saturates to a constant value smaller than $h_{\text{cross}}(L > 2R_g)$.

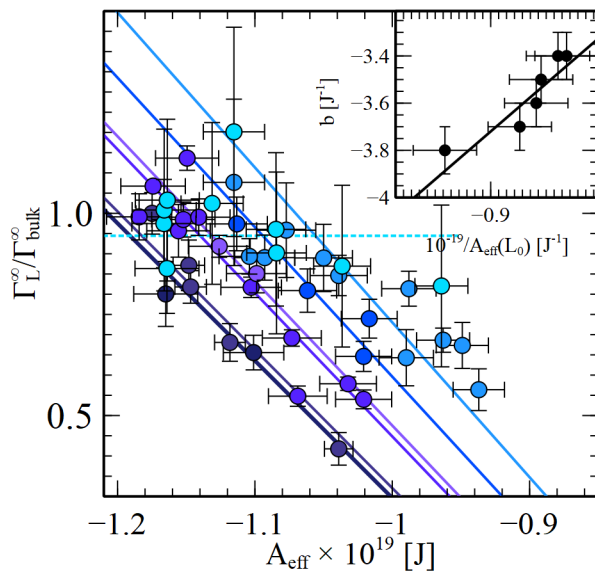


Fig. S11 - Normalized adsorbed amount as a function of the Hamaker constant for PS of different molecular weights (same color pattern as in Figures 1D and 2D). The different datasets, with exception of the values for the lowest molecular weight, are fitted to a linear expression of the form $\Gamma^\infty / \Gamma_{\text{bulk}}^\infty = a + b \times A_{\text{eff}}$. The value of a was obtained from the analysis of data Figure 2D, that is, imposing that for $A_{\text{eff}}=0$ the thickness of the spincoated layer equals 3.0 nm. Data for PS49 were not considered due to the excessive scattering, due to the relatively lower thickness of these films. In line with our reasoning, the slope b (see inset) is inversely proportional to $A_{\text{eff}}(L_0)$, which justifies the used of the scaling $\Gamma^\infty / \Gamma_{\text{bulk}}^\infty$ vs $A_{\text{eff}} / A_{\text{eff}}(L_0)$ in Figure 2D.

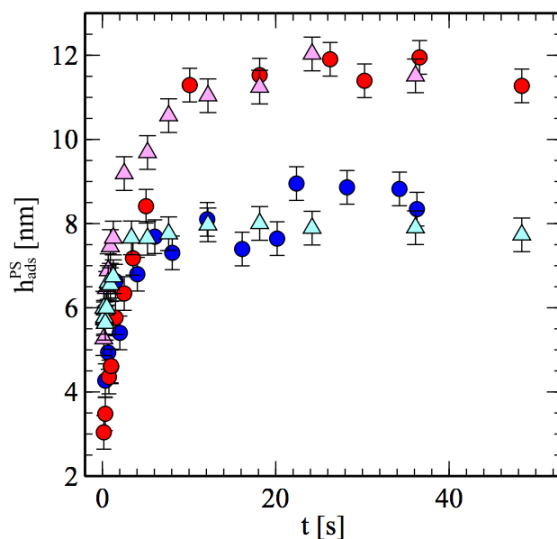












Fig. S12 - Comparison of the kinetics of adsorption in bilayer and monolayer systems having similar effective Hamaker constants ($\pm 0.5\%$). For the bilayer with $L_{\text{PS}} = 320$ nm and $L_{\text{PMMA}} = 25$ nm (pink triangles) and the monolayer with $L_{\text{PS}} = 250$ nm (red circles) $A_{\text{eff}} \approx -1.18 \times 10^{-19}$ J. For the bilayer with $L_{\text{PS}} = 320$ nm and $L_{\text{PMMA}} = 150$ nm (cyan triangles) and the monolayer with $L_{\text{PS}} = 103$ nm (blue circles) $A_{\text{eff}} \approx -1.14 \times 10^{-19}$ J.

Table S1. Supplementary information in polymer Materials and Properties.

<i>Symbol</i>	<i>Polymer</i>	<i>M_w [kDa]</i>	<i>PDI</i>	<i>Manufacturer</i>
	<i>PS</i>	<i>49</i>	<i>1.03</i>	<i>Polymer Laboratories</i>
	<i>PS</i>	<i>99</i>	<i>1.06</i>	<i>Polymer Source Inc.</i>
	<i>PS</i>	<i>325</i>	<i>1.03</i>	<i>Polymer Laboratories</i>
	<i>PS</i>	<i>488</i>	<i>1.05</i>	<i>Polymer Laboratories</i>
	<i>PS</i>	<i>560</i>	<i>1.11</i>	<i>Sigma-Aldrich</i>
	<i>PS</i>	<i>1040</i>	<i>1.03</i>	<i>Sigma-Aldrich</i>
	<i>PS</i>	<i>1460</i>	<i>1.04</i>	<i>Polymer Laboratories</i>
	<i>P4MS</i>	<i>72</i>	<i>2.61</i>	<i>Sigma-Aldrich</i>
	<i>PtBS</i>	<i>74</i>	<i>1.07</i>	<i>Polymer Source Inc.</i>
	<i>PMMA</i>	<i>350k</i>	<i>-</i>	<i>Sigma-Aldrich</i>

References

- (1) Bal, J. K.; Beuvier, T.; Unni, A. B.; Chavez Panduro, E. A.; Vignaud, G.; Delorme, N.; Chebil, M. S.; Grohens, Y.; Gibaud, A., Stability of Polymer Ultrathin Films (<7 nm) Made by a Top-Down Approach. *ACS Nano* **2015**, *9*, 8184-8193.
- (2) Richardson, H.; Carelli, C.; Keddie, J. L.; Sferrazza, M., Structural relaxation of spin-cast glassy polymer thin films as a possible factor in dewetting. *European Physical Journal E* **2003**, *12*, 437-440.
- (3) Richardson, H.; Sferrazza, M.; Keddie, J. L., Influence of the glass transition on solvent loss from spin-cast glassy polymer thin films. *European Physical Journal E* **2003**, *12*, S87-S91.
- (4) Housmans, C.; Sferrazza, M.; Napolitano, S., Kinetics of Irreversible Chain Adsorption. *Macromolecules* **2014**, *47*, 3390.
- (5) Braatz, M.-L.; Melendez, L. I.; Sferrazza, M.; Napolitano, S., Unexpected impact of irreversible adsorption on thermal expansion: Adsorbed layers are not that dead. *Journal of Chemical Physics* **2017**, *146*, 203304
- (6) de Silva, J. P.; Geoghegan, M.; Higgins, A. M.; Krausch, G.; David, M. O.; Reiter, G., Switching layer stability in a polymer bilayer by thickness variation. *Phys Rev Lett* **2007**, *98*, 267802.
- (7) Higgins, A. M.; Jones, R. A. L., Anisotropic spinodal dewetting as a route to self-assembly of patterned surfaces. *Nature* **2000**, *404*, 476-478.
- (8) Guiselin, O., Irreversible Adsorption of a Concentrated Polymer Solution. *Europh. Lett.* **1991**, *17*, 225-230.
- (9) Durning, C. J.; O'Shaughnessy, B.; Sawhney, U.; Nguyen, D.; Majewski, J.; Smith, G. S., Adsorption of poly(methyl methacrylate) melts on quartz. *Macromolecules* **1999**, *32*, 6772-6781.
- (10) Jenkins, F. A.; White, H. E., *Fundamentals of Optics 4th Ed.* McGraw-Hill Education: New York, 1981.
- (11) Palik, E., *Handbook of Optical Constants of Solids.* Academic Press: San Diego, 1998.
- (12) Burroughs, M. J.; Napolitano, S.; Cangialosi, D.; Priestley, R. D., Direct Measurement of Glass Transition Temperature in Exposed and Buried Adsorbed Polymer Nanolayers. *Macromolecules* **2016**, *49*, 4647-4655.
- (13) Simavilla, D. N.; Panagopoulou, A.; Napolitano, S., Characterization of Adsorbed Polymer Layers: Preparation, Determination of the Adsorbed Amount and Investigation of the Kinetics of Irreversible Adsorption. *Macromolecular Chemistry and Physics* **2017**, *219*, 201700303.
- (14) Fujii, Y.; Yang, Z.; Leach, J.; Atarashi, H.; Tanaka, K.; Tsui, O. K. C., Affinity of Polystyrene Films to Hydrogen-Passivated Silicon and Its Relevance to the Tg of the Films. *Macromolecules* **2009**, *42*, 7418-7422
- (15) Simavilla, D. N.; Huang, W. P.; Vandestruck, P.; Ryckaert, J.-P.; Sferrazza, M.; Napolitano, S., Mechanisms of Polymer Adsorption onto Solid Substrates. *ACS Macro Letters* **2017**, *8*, 975-979.
- (16) Boyd, R. H.; Smith, G. D., *Polymer Dynamics and Relaxation.* Cambridge University Press: Cambridge, 2007.

- (17) Panagopoulou, A.; Napolitano, S., Irreversible Adsorption Governs the Equilibration of Thin Polymer Films. *Phys Rev Lett* **2017**, *119*, 097801.
- (18) Wallace, W. E.; Tan, N. C. B.; Wu, W. L.; Satija, S., Mass density of polystyrene thin films measured by twin neutron reflectivity. *Journal of Chemical Physics* **1998**, *108*, 3798-3804.
- (19) Wallace, W. E.; Jacobsen, D. L.; Arif, M.; Ioffe, A., Application of neutron interferometry to the measurement of thin film density. *Applied Physics Letters* **1999**, *74*, 469.
- (20) De Virgiliis, A.; Milchev, A.; Rostiashvili, V. G.; Vilgis, T. A., Structure and dynamics of a polymer melt at an attractive surface. *European Physical Journal E* **2012**, *35*, 97.
- (21) Israelachvili, J. N., *Intermolecular and surface forces* Academic Publisher: San Diego, 2011.
- (22) Lawnik, W. H.; Findenegg, G. H., Ellipsometric studies of wetting on low-energy surfaces. *Berichte der Bunsengesellschaft für physikalische Chemie* **1994**, *98*, 405-408.
- (23) Gregory, J., Approximate expressions for retarded van der waals interaction. *J. Colloid Interface Sci.* **1981**, *83*, 138-145.
- (24) Casimir, H. B. G.; Polder, D., The Influence of Retardation on the London-van der Waals Forces. *Physical Review E* **1948**, *73*, 360.